Technical note: Quantifying the Nitrogen Isotope Difference between Ammonium in the Atmosphere and Ammonia Emitted from Sources

Chongguo Tian[1,2,*], Xuehua Yin[2,3], Xuena Yang[1], Xiaoxia Yu[1], Zhengjie Li[4], Zheng Zong[5], Xinpeng Tian[2], Yuchen Li[2,3], Roland Kallenborn[6], Yi-Fan Li [7]

[1] Key Laboratory of Land and Sea Ecological Governance and Systematic Regulation, Shandong Academy for Environmental Planning, Jinan, 250101, P.R. China
[2] Shandong Key Laboratory of Coastal Environmental Processes, CAS Key Laboratory of Coastal Environmental Processes and Ecological Remediation, Yantai Institute of Coastal Zone Research, Chinese Academy of Sciences, Yantai 264003, P.R. China
[3] University of Chinese Academy of Sciences, Beijing, 100049, P.R. China
[4]National Engineering Laboratory for Applied Technology of Forestry & Ecology in Southern China, College of Biological Science and Technology, Central South University of Forestry and Technology, Changsha, Hunan 410004, China
[5] Environment Research Institute, Shandong University, Qingdao 266237, P.R. China
[6] Norwegian University of Life Sciences, Faculty of Chemistry, Biotechnology and Food Sciences, Christian Magnus Falsens vei 18, 1433, As, Norway
[7] International Joint Research Center for Persistent Toxic Substances (IJRC-PTS), State Key Laboratory of Urban Water Resource and Environment, Harbin Institute of Technology, Harbin 150090, P.R. China

Correspondence to: Chongguo Tian (cgtian@yic.ac.cn)

Abstract. The difference ($\delta^{15}N_{4a\text{-}3s}$) in nitrogen isotopes ($\delta^{15}N$) between NH_4^+ and source-emitted NH_3 is a crucial factor influencing the source apportionment of atmospheric NH_4^+. This $\delta^{15}N_{4a\text{-}3s}$ is mainly due to isotopic fractionation during NH_3-NH_4^+ gas-particle conversion and atmospheric deposition. The impact of isotope fractionation on $\delta^{15}N_{4a\text{-}3s}$ had been well quantified by simplified method, but that of atmospheric deposition had often been overlooked. This study developed a model to assess $\delta^{15}N_{4a\text{-}3s}$ variations by considering both the atmospheric deposition and isotope fractionation. The results of six model scenarios showed the difference between $\delta^{15}N_{4a\text{-}3s}$ values under both influences and under isotope fractionation alone increased with the rise of f (the molar fraction of NH_4^+ to NH_x in the atmosphere). At 20°C, when f = 0.9, the maximum gap could reach 10.7%. $\delta^{15}N_{4a\text{-}3s}$ was insensitive to NH_3 and NH_4^+ deposition ratio, NH_4^+ generation ratio, and temperature, but it was sensitive to f. A prediction function for $\delta^{15}N_{4a\text{-}3s}$ was constructed and applied to atmospheric NH_4^+ source apportionment in the Yellow River Delta and Changsha. Compared with the simplified method, the fitted equation provided a more reasonable estimate of the contribution of agricultural sources and non-fossil fuel sources. The constructed equation could be used for tracing atmospheric NH_4^+ origin, thus improving the accuracy of atmospheric NH_4^+ source apportionment.

1. Introduction

Ammonia (NH_3) is the primary alkaline gas in the atmosphere, and its cycle plays a crucial role in the geological and biological nitrogen cycles on Earth's surface. NH_3 can neutralize atmospheric acids such as sulfuric acid (H_2SO_4), nitric acid (HNO_3), and hydrochloric acid (HCl), forming particulate ammonium (NH_4^+) aerosols. This process deteriorates air quality and affects the acidity of airborne particulate matter, precipitation, and cloud water (Ianniello et al., 2010; Pan et al., 2016; Chang et al., 2019b). NH_3 and NH_4^+ (collectively abbreviated as NH_x) are deposited back to the surface through dry and wet deposition processes. Excess NH_x in the atmosphere not only leads to eutrophication of terrestrial

and aquatic ecosystems and threatens biodiversity, but also increases public health risks (Bobbink et al., 2010; Liu et al., 2019; Tan et al., 2020; Bouwman et al., 2002). In recent decades, rapid industrialization, urbanization, and agricultural development have significantly increased NH_3 emission worldwide, particularly in Asia, Africa, and South America. This resulted in a substantial rise in severe haze events and eutrophication risks in these regions (Zhao et al., 2017; Bouwman et al., 2002; Kim et al., 2011). In order to develop effective strategies to reduce NH_x levels in the atmosphere, source apportionment of NH_x has garnered considerable attention as a foundational research focus in recent years (Behera et al., 2013; Shen et al., 2011; Hu et al., 2014; Schiferl et al., 2016; Sun et al., 2016).

Numerous methods have been developed and used to trace sources of NH_x in the atmosphere. Among these, the utilization of the stable nitrogen isotopic composition of gaseous NH_3 (δ^{15}N-NH_3) or aerosol NH_4^+ (δ^{15}N-NH_4^+) has emerged as a highly promising tool for source apportionment of NH_3 in the atmosphere (Gu et al., 2025; Elliott et al., 2019). However, it is important to note that neither aerosol δ^{15}N-NH_4^+ nor gaseous δ^{15}N-NH_3 can be directly used for this purpose alone. This is because their isotopic values do not correspond directly to the δ^{15}N-NH_3 of mixed NH_3 emissions from various sources (Zhang et al., 2020). The discrepancy arises from nitrogen isotope exchange between NH_3 and NH_4^+ in the atmosphere (Walters et al., 2019; Kawashima and Ono, 2019). Observations typically show higher δ^{15}N values in NH_4^+ compared to NH_3, which can be attributed to equilibrium isotopic fractionation (Walters et al., 2019). The mass and isotope balance for NH_x in the atmosphere is given by the following equation:

$$f\delta^{15}N-NH_4^+ + (1-f)\delta^{15}N-NH_3 = \delta^{15}N-NH_x, \quad (1)$$

where f is the molar fraction of NH_4^+ to NH_x in the atmosphere, and δ^{15}N-NH_4^+, δ^{15}N-NH_3 and δ^{15}N-NH_x are the isotopic composition of NH_4^+, NH_3 and NH_x in the atmosphere, respectively. After the introduction of the isotopic fractionation factor (α) between NH_4^+ and NH_3, the Eq. (1) can be rewritten as:

$$\delta^{15}N-NH_4^+ = \frac{\alpha}{1+(\alpha-1)f}\delta^{15}N-NH_x + \frac{1000(\alpha-1)(1-f)}{1+(\alpha-1)f}, \quad (2)$$

Because the coefficients of $\frac{\alpha}{1+(\alpha-1)f}$ and $1+(\alpha-1)f$ are approximately equal to one, the Eq. (1) is often simplified as:

$$\delta^{15}N_{4a-3x} = \delta^{15}N-NH_4^+ - \delta^{15}N-NH_x = 1000(\alpha-1)(1-f), \quad (3)$$

where $\delta^{15}N_{4a-3x}$ is difference between δ^{15}N-NH_4^+ and δ^{15}N-NH_x in the atmosphere. The difference is often used to correct the δ^{15}N of NH_4^+ in the atmosphere, so as to apportion sources of NH_4^+ (Pan et al., 2018; Pan et al., 2016; Chang et al., 2016). The underlying assumption is that the atmosphere is a well-mixed closed system, implying that δ^{15}N-NH_x values in the atmosphere are equivalent to those of the δ^{15}N-NH_3 emitted from various sources. However, it is a well-established fact that both NH_3 and NH_4^+ can exit the atmosphere through deposition processes. These deposition processes may introduce substantial discrepancies between the δ^{15}N-NH_x values observed in the atmosphere and the δ^{15}N-NH_3 values emitted from sources. This bias could further compromise the accuracy of δ^{15}N-based source apportionment (Zhang et al., 2020).

To more accurately identify the source of atmospheric NH_x, this study develops a model to quantify the difference in δ^{15}N-NH_4^+ in the atmosphere and source-emitted δ^{15}N-NH_3 ($\delta^{15}N_{4a\text{-}3s}$) under combined atmospheric deposition and isotope fractionation. It should be noted that the model primarily addresses the isotopic mass balance shift induced by deposition processes, rather than detailed chemical mechanisms. The objectives of this study are (1) to understand the variation pattern of $\delta^{15}N_{4a\text{-}3s}$ and the key influencing factors, (2) to construct a fitting equation for the $\delta^{15}N_{4a\text{-}3s}$ and the key influencing factors used for NH_4^+ source apportionment, and (3) to evaluate the application effects of the fitted equation in the source apportionment of NH_4^+ through practical examples.

2. Methods and Theory

2.1 Model Development

Similar to the Eq. (3), the $\delta^{15}N_{4a\text{-}3s}$ could be calculated as follows:

$$\delta^{15}N_{4a-3s} = (\delta^{15}N-NH_4^+ - \delta^{15}N-NH_{3s}) = 1000(\alpha-1)(1-f), \quad (4)$$

where δ^{15}N-NH_{3s} is the nitrogen isotope of NH_3 from various types of sources and other items are the same as that in Eq. (1) and (2). The equation indicates that the variation in $\delta^{15}N_{4a\text{-}3s}$ depends on the change of α, *f* and δ^{15}N-NH_x. Consequently, the core objective of this model is to iteratively update α, *f* and δ^{15}N-NH_3 in an open system that accounts for the combined effects of NH_3/NH_4^+ conversion and sedimentation, and ultimately to determine the steady-state $\delta^{15}N_{4a\text{-}3s}$.

Firstly, the parameter α is defined as (δ^{15}N-NH_4^++1000)/ (δ^{15}N-NH_3+1000) (Coplen, 2011). This value of α could be empirically determined by fitting experimental data (Urey, 1947; Li et al., 2012) and computational quantum chemistry method (Walters et al., 2019) based on the ambient temperature. The present study used the computational quantum chemistry method (Walters et al., 2019) to calculate the α values as the following method:

$$1000(\alpha-1) = \frac{12522}{T(K)} - 11.31 \ , \quad (5)$$

where T is the ambient temperature (in Kelvin). The values of *f* and δ^{15}N-NHx vary synchronously during the iteration. Next, the continuous variations in atmospheric NH_3 and NH_4^+, together with their deposition processes, were discretized. Assuming the atmosphere is a well-mixed open system, three processes occur simultaneously at each iteration step: partial conversion of NH_3 to NH_4^+, deposition loss of NH_3, and deposition loss of NH_4^+. Accordingly, the mass fractions of atmospheric NH_3 and NH_4^+, as well as their deposited fractions, can be expressed as follows:

$$\begin{aligned} [NH_{3a}]^t &= (1-G_4-D_3)[NH_{3a}]^{t-1} \\ [NH_{4a}^+]^t &= G_4[NH_{3a}]^{t-1} + (1-D_4)[NH_{4a}^+]^{t-1} \\ [NH_{3d}]^t &= D_3[NH_{3a}]^{t-1} \\ [NH_{4d}^+]^t &= D_4[NH_{4a}^+]^{t-1} \end{aligned} \ , \quad (6)$$

where G_4, D_3 and D_4 represent the transformation ratio of NH_3 to NH_4^+, and the deposition ratio of NH_3 and the deposition ratio of NH_4^+, respectively. All three are dimensionless parameters defined for a single iteration step. The superscript t denotes the iteration index, starting from t=1, and does not represent a specific physical duration. The model is iterated to steady state, and the resulting steady-state $\delta^{15}N_{4a\text{-}3s}$ is

taken as the model output. [NH_{3a}] and [NH_{4a}^+] are the mass fractions of atmospheric NH_3 and NH_4^+, whereas [NH_{3d}] and [NH_{4d}^+] are the corresponding deposited fractions in that iteration step. The molar fraction of NH_4^+ in NH_x at iteration step t can then be calculated as follows：

$$f^t = \frac{[NH_{4a}^+]^t}{[NH_x]^t} = \frac{[NH_{4a}^+]^t}{[NH_{4a}^+]^t + [NH_{3a}]^t}, \quad (7)$$

where $[NH_x]^t$ is the mass fraction of NH_x in the atmosphere at the t^{th} time interval, and the meanings of other items are the same as those in Eq. (6). Furthermore, given that α and f are known, the values of [δ^{15}N-NH_4^+] and [δ^{15}N-NH_3] at the t^{th} time interval can be expressed as:

$$\begin{aligned} [\delta^{15}N - NH_{4a}^+]^t &= [\delta^{15}N - NH_x]^{t-1} + 1000(\alpha - 1)(1 - f^{t-1}) \\ [\delta^{15}N - NH_{3a}]^t &= [\delta^{15}N - NH_x]^{t-1} - 1000(\alpha - 1)f^{t-1} \end{aligned}, \quad (8)$$

It can be assumed that δ^{15}N values of NH_3 and NH_4^+ ([δ^{15}N-NH_{4d}^+] and [δ^{15}N-NH_{3d}]) deposited to the surface are equal to δ^{15}N-NH_3 and δ^{15}N-NH_4^+ in the atmosphere at the t^{th} time interval, respectively, as the following:

$$\begin{aligned} [\delta^{15}N - NH_{4d}^+]^t &= [\delta^{15}N - NH_{4a}^+]^t \\ [\delta^{15}N - NH_{3d}]^t &= [\delta^{15}N - NH_{3a}]^t \end{aligned}, \quad (9)$$

This assumption implies that the deposition process itself does not introduce additional isotopic fractionation; its effect is limited to altering the mass composition of the remaining NH_x in the atmosphere, without further altering the isotopic values of the corresponding components. It should be noted that this assumption is not directly substituted into Eq. (4) to calculate $\delta^{15}N_{4a\text{-}3s}$, but rather indirectly influences δ^{15}N-NH_x and f in Eq. (4) by altering the mass fraction and isotopic composition of the remaining atmospheric NH_x, thereby ultimately affecting $\delta^{15}N_{4a\text{-}3s}$.

Subsequently, using Eq. (10), the overall isotopic composition of atmospheric NH_x at the t^{th} iteration step, [δ^{15}N-NH_x]^t, can be further derived. This quantity serves both as a characterisation of the system's isotopic state at the current step and as an input for the next iteration, continuing to participate in the calculations. Correspondingly, [δ^{15}N-NH_x] in the atmosphere at the t^{th} time interval can be written as:

$$[\delta^{15}N - NH_x]^t = f^t[\delta^{15}N - NH_{4a}^+]^t + (1 - f^t)[\delta^{15}N - NH_{3a}]^t, \quad (10)$$

Thus, Equations (6)-(10) together form an iterative framework for an open system that continuously updates the mass fractions of NH_3 and NH_4^+ and their isotopic compositions. The initial conditions of the model are set as follows: at t = 1, [δ^{15}N-NH_x] = [δ^{15}N-NH_{3s}], i.e. the isotopic composition of atmospheric NH_x at the initial time of the system is equal to that of the source-emitted NH_3. Thereafter, the model is solved iteratively in the following sequence:

(1) Set up source [δ^{15}N-NH_{3s}];
(2) Set up G_4, D_3, and D_4 to calculate [NH_{3a}], [NH_{3d}], [NH_{4a}^+] and [NH_{4d}^+] from Eq. (6);
(3) Calculate f from Eq. (7);
(4) Input T to calculate α from Eq. (5);
(5) Calculate [δ^{15}N-NH_{4a}^+], [δ^{15}N-NH_{3a}], [δ^{15}N-NH_{4d}^+] and [δ^{15}N-NH_{3d}] from Eq. (8) and (9);
(6) Calculate [δ^{15}N-NH_x] from Eq. (10);
(7) Calculate $\delta^{15}N_{4a\text{-}3s}$ from Eq. (4).

The model was developed by R 4.1.3 software.

2.2 Parameter Identification

As described in the previous section, the value of $\delta^{15}N_{4a\text{-}3s}$ could be predicted by the developed model if the values of G_4, D_3, D_4, T, and [δ^{15}N-NH_{3s}] were available. The G_4, D_3, and D_4 had strong spatiotemporal variability, primarily driven by the difference in the content and composition of acidic gases in the atmosphere, as well as the variation of surface roughness, wind speed, and etc (Baek and Aneja, 2004; Schrader and Brummer, 2014). This is a systematic project that cannot be validated experimentally by an article. So, here we constructed six simulation scenarios to assess the extent to which changes in the three parameters affected the simulation results of $\delta^{15}N_{4a\text{-}3s}$ as listed in Table 1.

These six simulation scenarios were composed of combining G_4 being equal to 0.5 times, 1.0 times and 2.0 times D_3, as well as D_4 being 0.2 times and 0.5 times D_3 respectively. The detailed basis for this proportion setting could be found in the Text S1 and Tables S1-S2 in the Supporting Information (SI). Briefly, the G_4 is mainly attributed to the comprehensive neutralization reaction ratio of ammonia (NH_3) with acid gases (sulfuric acid (H_2SO_4), nitric acid (HNO_3) and hydrochloric acid (HCl)) in the atmosphere (Baek and Aneja, 2004). Under normal atmospheric conditions, the relatively abundant acidic gas in the atmosphere could make the G_4 faster, and the G_4 between NH_3 and H_2SO_4 was faster than that of NH_3 with HNO_3 and HCl, as listed in Text S1 of SI (Schrader and Brummer, 2014). To evaluate the impact of varying acid-gas concentrations, we established three G_4 levels: 0.5× D_3 (low acid-gas content), 1.0× D_3 (moderate acid-gas content), and 2.0× D_3 (high acid-gas content). Surface roughness is an important parameter affecting the ratio of atmospheric deposition of NH_3 and NH_4^+, with a general pattern of decreasing deposition ratio from mountainous regions to flat terrain areas (Zhang et al., 2001). Numerous studies had also shown that the D_4 was significantly lower than D_3 in the atmosphere (Shen et al., 2009). Therefore, we set two levels for D_4, one was 0.2×D_3 and the other was 0.5×D_3, representing the deposition differences in flat regions and mountainous areas, respectively.

Table 1. Parameter settings, characteristics and representative regions of the six model scenarios.

	G_4	D_4	Characteristics and representative regions
MS1	0.5D_3	0.2D_3	less acidic gas and flat surfaces, open oceans.
MS2	0.5D_3	0.5D_3	less acidic gas and rough surfaces, mountainous forests.
MS3	1.0D_3	0.2D_3	moderate acidic gas and flat surfaces, plain background regions.
MS4	1.0D_3	0.5D_3	moderate acidic gas and rough terrains, mountainous background regions.
MS5	2.0D_3	0.2D_3	higher acidic gases and flat terrains, plain cities.
MS6	2.0D_3	0.5D_3	higher acidic gas and rough terrains, mountainous cities.

A total of five temperature levels of -10°C, 0°C, 10°C, 20°C, 30°C were set for the above six simulation scenarios. In addition, the [δ^{15}N-NH_{3s}] was set to 0 ‰ in these simulations.

2.3 Sensitivity Analysis

Sensitivity analysis is a statistical technique used to quantify the extent to which variations in different inputs influence the variability of the outputs. In present study, sensitivity analysis was conducted to examine the impact of individual parameters on the $\delta^{15}N_{4a\text{-}3s}$ values. This analysis was achieved by assessing how sensitive the model was to alterations in its input parameters. To do this, the model was run with each parameter individually scaled to 0.9 and 1.1 times its original value (Cao et al., 2007). The evaluation involved computing sensitivity coefficients (*SC*), which quantify the relative changes in the primary output estimates in response to changes in the input parameters, as outlined below:

$$SC = abs\left(\frac{OUT_{1.1}-OUT_{0.9}}{0.2\times OUT_{1.0}}\right), \quad (11)$$

where $OUT_{1.1}$, $OUT_{1.0}$, and $OUT_{0.9}$ are the model output results when the input parameter is 1.1, 1.0, and 0.9 times of its original value, respectively. The sensitivity of various parameters can be directly compared because the *SC* values obtained through Eq. (11) are dimensionless. The absolute magnitude of *SC* represents the extent to which input parameters affect the output results. Furthermore, the positive or negative sign of *SC* reveals the direction of this influence: positive values signify that an increase in input parameters leads to an increase in output results, whereas negative values imply the opposite relationship (Cao et al., 2007; Dong et al., 2010).

3. Results and Discussion

3.1 The Variation in $\delta^{15}N_{4a\text{-}3s}$ with *f*

Figure 1 shows the variation of $\delta^{15}N_{4a\text{-}3s}$ with respect to the *f* value at temperatures of -10°C, 0°C, 10°C, 20°C, and 30°C, respectively, by the six model scenarios. In order to aid in comparisons, Fig.1 also displays that the change in $\delta^{15}N_{4a\text{-}3x}$ obtained using Eq. (4), which can be thought of as the $\delta^{15}N_{4a\text{-}3s}$ value calculated using the simplified method. Under different temperature conditions, the six simulation scenarios all obtained similar change characteristics, that is, the $\delta^{15}N_{4a\text{-}3s}$ value decreased with the increase of *f* value.

The following took the results at 20°C as an example to further illustrate. Specifically, when *f* was 0.1, the $\delta^{15}N_{4a\text{-}3s}$ values across the six simulated scenarios average around 28.8‰. Conversely, when *f* reached 0.9, the $\delta^{15}N_{4a\text{-}3s}$ values decreased to a range of 5.89-14.0‰. Among the six model scenarios, the variation in $\delta^{15}N_{4a\text{-}3s}$ values was narrower in regions with lower generation ratios (G_4) and deposition ratios (D_4) of NH_4^+(such as MS1 and MS2), whereas it was broader values in regions with higher ratios (such as MS5 and MS6). The finding suggested that there was a minor fluctuation in $\delta^{15}N_{4a\text{-}3s}$ values in areas with less acidic gas and flat landscapes, like flat land surfaces and open oceans, whereas a more significant variation was observed in $\delta^{15}N_{4a\text{-}3s}$ values in regions characterized by higher acidic gas levels and rugged terrains, such as mountainous cities with high air pollution load.

The change in $\delta^{15}N_{4a\text{-}3s}$ values calculated by the simplified method was larger than those $\delta^{15}N_{4a\text{-}3s}$ values yielded by all six model scenarios, and their difference was a gradual increase as *f* values increase. The difference indicated that when the simple method was used for source apportionment of NH_4^+ in the atmosphere, the deviation would be larger with the increase of *f* value. This phenomenon originated from

NH_3 exhibiting a higher deposition rate compared to NH_4^+(Behera and Sharma, 2011, 2012), which results in a greater proportion of NH_x components with lower $\delta^{15}N$ values being removed from the atmosphere. Consequently, the $\delta^{15}N$-NH_x in the atmosphere gradually increased. When using the $\delta^{15}N_{4a-3s}$ values calculated by the simplified method to correct the $\delta^{15}N$ of NH_4^+ for the purpose of apportioning sources of NH_4^+, overcorrection may occur, leading to an overestimation of the contribution proportion of NH_3 emission sources with relatively negative $\delta^{15}N$ values, like non-agricultural sources (e.g., vehicle exhaust and NH_3 slip) (Zong et al., 2023; Feng et al., 2023). The larger $\delta^{15}N_{4a-3s}$ value was in the case of lower ambient temperature, indicating that the difference between $\delta^{15}N_{4a-3s}$ calculated by the model scenarios and the simplified method had more obvious influence on the source apportionment of NH_4^+ in the northern cold region and the winter period when the temperature was lower(Sun et al., 2021).

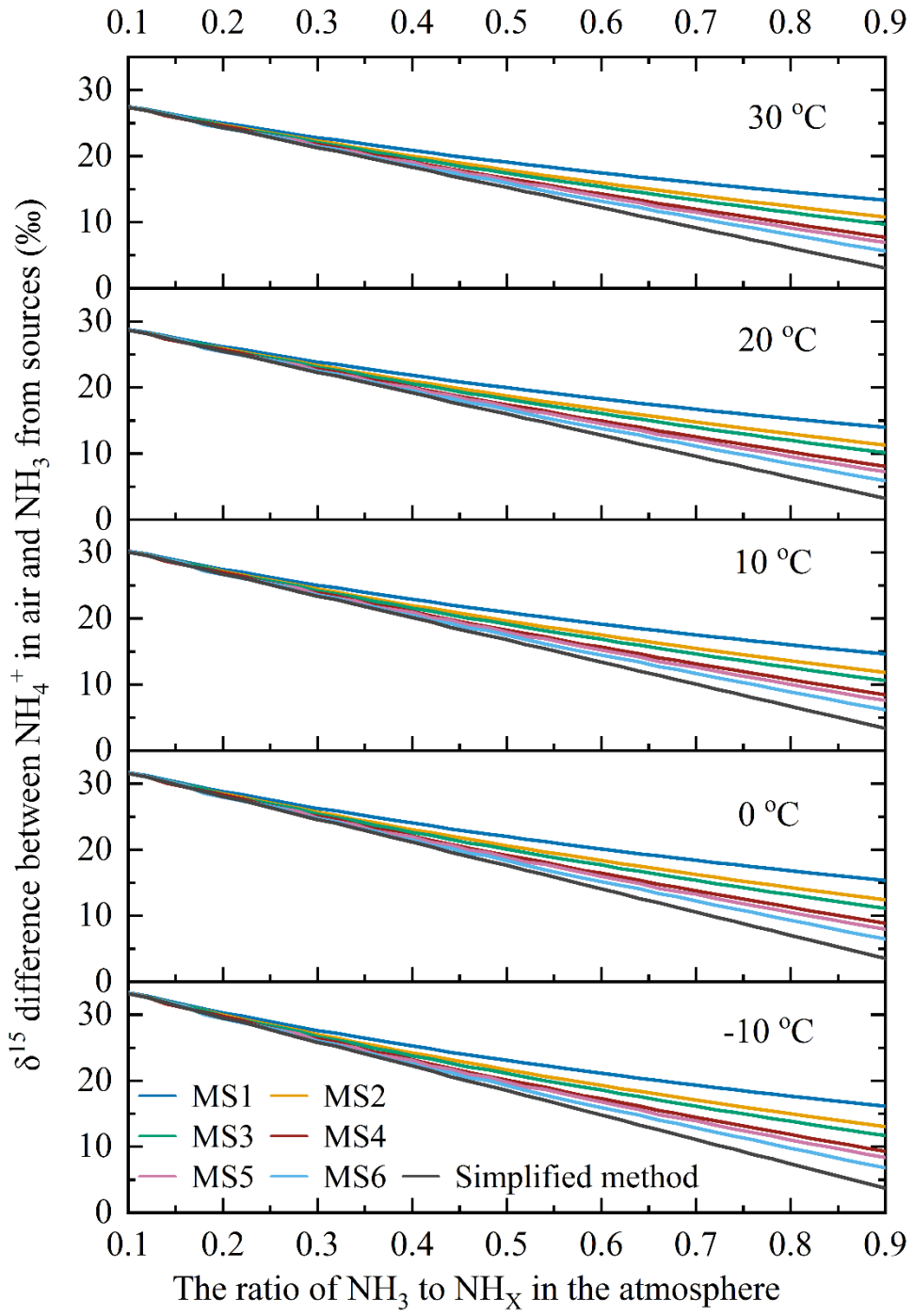

Figure 1. The variation in $\delta^{15}N_{4a-3s}$ with *f* at -10°C, 0°C, 10°C, 20°C, and 30°C simulated by the six model scenarios and the simplified method. (note: $\delta^{15}N_{4a-3s}$ is the difference between $\delta^{15}N\text{-}NH_4^+$ in the atmosphere and $\delta^{15}N\text{-}NH_3$ emitted from sources, MS1-MS6 are the six model scenarios as listed in Table 1, the simplified method is showed in Eq. (4)).

3.2 Sensitivity of $\delta^{15}N_{4a-3s}$ to Input Parameters

The sensitivity coefficients of each input parameters (D_3, D_4, G_4, and T) to the $\delta^{15}N_{4a-3s}$ values at 20°C were calculated by using Eq. (11) across the six model scenarios (see Fig. 2). The sensitivity coefficient of D_3 variation on the simulation results ranged between 2.55×10^{-5} and 9.32×10^{-2}. The sensitivity coefficient of D_4 and G_4 variations on the $\delta^{15}N_{4a-3s}$ ranged respectively from 1.77×10^{-5} to 0.474 and from 3.62×10^{-4} to 0.494, showing a similar variation signature, which intensified as the value of *f* increases. Additionally, the range of variation in D_4's sensitivity coefficient also widened as the value of *f* increased. However, G_4 did not exhibit this characteristic. The variation range of the sensitivity coefficient of temperature (T) variation on the simulation results was narrow, falling between 0.092 and 0.094, and this influence diminished as the value of *f* increased. Generally, the sensitivity coefficient exceeding 0.5 is considered that the corresponding input parameter has a sensitive influence on the output result (Cao et al., 2007). It suggested that the influence of each individual input parameter on the simulation output result ($\delta^{15}N_{4a-3s}$) did not show obvious sensitivity in the six model scenarios.

In fact, the degree to which input parameters affect the simulation results is not only related to the sensitivity coefficient evaluated based on a single input parameter, but also to the synergistic effect of changes in all input parameters (Wang et al., 2023). In this model simulation, the changes in the $\delta^{15}N_{4a-3s}$ and *f* were the results of the input parameter changes. Taking *f* as a comprehensive input parameter of D_3, D_4, G_4, and T, the sensitivity of *f* to output results based on the six simulation scenarios was calculated by formula (11). The variation range of the calculated corresponding sensitivity coefficient with *f* is also shown in Fig. 2. The variation characteristic of this sensitivity coefficient is similar to that of the input parameter D_4, showing that the variation range becomes larger and larger with the increase of *f*. When the *f* value was greater than 0.32, the maximum of the sensitivity coefficients obtained by the six simulation scenarios began to be greater than 0.5, that is, the changes in the input parameters (*f*) were generally considered to have sensitive effects on the output results ($\delta^{15}N_{4a-3s}$) (Cao et al., 2007). The maximum range of variation of this sensitivity coefficient was from 0.831 to 3.90 when the *f* value reached 0.9.

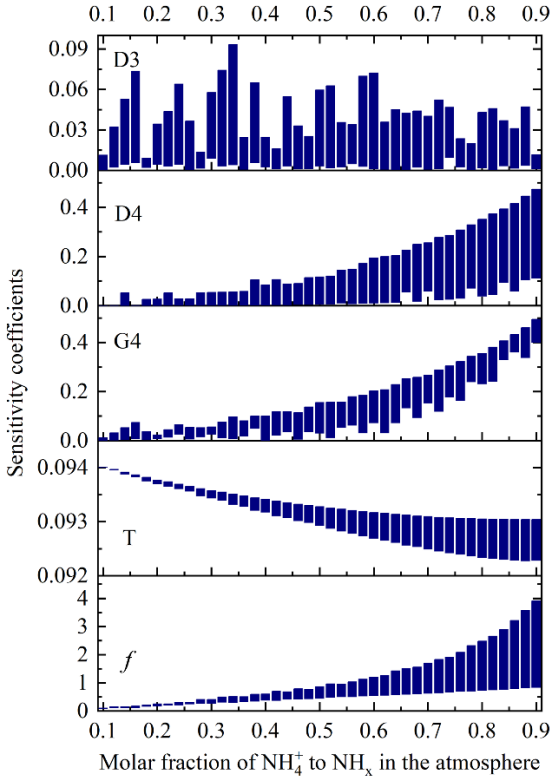

Figure 2. The variation range of sensitivity coefficients of input parameters to the $\delta^{15}N_{4a\text{-}3s}$ values at 20°C obtained from six simulation scenarios.

These ranges of sensitivity coefficients were generated by six simulation scenarios. To better understand them, the sensitivity coefficients of *f* to output results ($\delta^{15}N_{4a\text{-}3s}$) derived from the six simulation scenarios are shown in Fig. S1 of SI. The simulation results of MS1 scenario had the lowest sensitivity to *f*, while the simulation results of MS6 scenario had the highest sensitivity to *f*, indicating that large D_4 and G_4 had a greater impact on the simulation results. The finding also indicated that in some urban areas with more acidic gases, especially in mountainous areas, more attention should be paid to the influence of *f* changes on the source apportionment of NH_4^+ in the atmosphere.

3.3 Construction of the Prediction Function for $\delta^{15}N_{4a\text{-}3s}$

As mentioned earlier, $\delta^{15}N_{4a\text{-}3s}$ is generally calculated using Eq. (3) when apportioning sources of NH_4^+ in the atmosphere. The independent variable of this equation included the key influencing parameter *f*. Based on the form of Eq. (3) and the calculation results of the $\delta^{15}N_{4a\text{-}3s}$ values, we constructed a calculation function for the $\delta^{15}N_{4a\text{-}3s}$ values through nonlinear regression. The form of this nonlinear function is shown in Eq. (12). The coefficient values of B, C, and D in the equation were iteratively fitted for six simulation scenarios. During the fitting process, each simulation scenario took into account different temperature conditions, including -10°C, 0°C, 10°C, 20°C, and 30°C.

$$\delta^{15}N_{4a-3s} = 1000(\alpha^B - 1)(1 - f^C) + D\ , \quad (12)$$

Table 2 lists the iterative fitting values of the coefficients B, C, and D in Eq. (12) for the six model scenarios (MS1−MS6), as well as the determination coefficient (r^2) and sum of squares error (SSE), which were often used to evaluate the fitting effect (Sun et al., 2023; Xu, 2017). Figure S2 and Figure S3 of SI show the comparison plots and scatter plots of the $\delta^{15}N_{4a\text{-}3s}$ values calculated by the six fitted

equations against the six model scenarios (MS) simulated by the developed model. The coefficients B and C are both greater than 0 and less than 1, and the two coefficients gradually increase from MS1 to MS6, indicating that the Eq. (12) for model scenarios from MS1 to MS6 approaches from nonlinear to linear. The determination coefficients obtained from the regression of the six fitting equations with the simulation results range from 0.967 to 0.998, indicating that these equations can fit the calculated $\delta^{15}N_{4a-3s}$ values quite well (see Fig. S3 of SI). As shown in Fig. S2 of SI, the maximum deviation between the $\delta^{15}N_{4a-3s}$ values obtained from the fitting equation and those calculated by the model occurs in the model scenario of MS1. Under -10°C condition, the deviation reached its maximum value (1.82‰) when the *f* value was 0.9. This largest deviation was also significantly smaller than the variation range of $\delta^{15}N$ values of NH_3, which emitted from various types of sources used in the source apportionment of atmospheric NH_4^+ (Gu et al., 2022; Zhang et al., 2023; Feng et al., 2022; Li et al., 2023). This indicated that these fitting equations would not significantly increase the uncertainty of the source-resolved assessment of NH_4^+ in the atmosphere when they were used.

3.4 Comparison of Source Apportionment of Atmospheric NH_4^+ in Two Case Studies

In order to evaluate the fitting equations as mentioned above using monitoring data, we conducted a source apportionment simulation of NH_4^+ again using the atmospheric $\delta^{15}N$-NH_4^+ in the Yellow River Delta in the summers of 2013 and 2021. Apart from the difference in the method of calculating $\delta^{15}N_{4a-3s}$ values, the model, input data, etc. were consistent with those reported in our previous study(Zong et al., 2023). Briefly, the Bayesian mixing model (MixSIAR) developed by the R language was used for the source apportionment of NH_4^+. Four main types of NH_3 emission sources, including fertilizer use (−25.21 ± 9.43 ‰), livestock waste (−16.14 ± 7.98 ‰), vehicle exhaust (+6.62 ± 1.89 ‰), and NH_3 slip (−7.12 ± 7.62 ‰) (Table S3), were considered in the model. In the previous study, we used equation (3) (termed as simplified method) to calculate the $\delta^{15}N_{4a-3s}$ values. In this simulation, we used the MS1 fitting equation to calculate the $\delta^{15}N_{4a-3s}$ values. This is because these atmospheric particulate matter samples were collected at the Yellow River Delta Ecological Research Station of Coastal Wetland, Chinese Academy of Sciences (37°45′N, 118°59′E). The Yellow River Delta is an alluvial plain formed by the Yellow River, featuring a very flat terrain (Li et al., 2022; Zhang et al., 2025). Additionally, there are no obvious emission sources from industrial, transportation, and agricultural activities around the sampling site. Many studies regarded this sampling site as an atmospheric background point in North China (Zong et al., 2015; Sui et al., 2015), which met the characteristics of low pollution and a flat terrain in the MS1 scenario. Moreover, the deviation between the $\delta^{15}N_{4a-3s}$ values calculated by the MS1 method and the simplified method is the largest as shown in Fig. 1, which is more conducive to our evaluation of the degree of difference between the source apportionment results obtained by the two methods.

Table 2. The regression coefficients calculated with $\delta^{15}N_{4a-3s}$ as the dependent variable and the isotopic fractionation factor (α) and the molar fraction of NH_4^+ to NH_x in the atmosphere (*f*) as independent variables.

	B	C	D	r^2	SSE
MS1	0.654	0.728	12.534	0.967	150

MS2	0.748	0.775	9.468	0.986	86.6
MS3	0.790	0.793	8.138	0.991	64.3
MS4	0.854	0.843	5.747	0.996	32.2
MS5	0.881	0.862	4.787	0.997	23.6
MS6	0.928	0.882	3.267	0.998	11.6

Note: r^2 is the determination coefficient and SSE is sum of squares error.

For ease of comparing the differences, we summarized both the reported previously results and the findings of this study in Fig. 3. For the sources of atmospheric NH_4^+ in 2013, the most noticeable difference between the two source apportionment methods was the significant increase in the contribution proportion of fertilizer application (from 32.9% using the simplified method to 68.8% using the fitting equation method) and the corresponding NH_4^+ concentration (from 1.33 μg/m^3 using the simplified method to 2.78 μg/m^3 using the fitting method). The contributions of the other three emission sources decreased to varying degrees. When we previously used the simplified method for NH_4^+ source apportionment, we found that literature reports indicated similar annual NH_3 emissions from fertilizer application and livestock farming in North China, and even in Shandong Province(Zhang et al., 2010). Based on this evidence, we determined that agricultural sources were the main contributors to atmospheric NH_4^+ in the Yellow River Delta region in 2013, accounting for 67.4% (Zong et al., 2023). Recent NH_3 emission inventory results for Shandong showed that farmland fertilizer application sources were closer to the Yellow River Delta than livestock farming sources (Zhu et al., 2024), and that farmland emissions in summer are significantly higher than those from livestock farming (Li et al., 2021). This was consistent with the higher contribution proportion of fertilizer application to atmospheric NH_4^+ concentration obtained using the fitting equation method in this study, with the proportion also increasing correspondingly to 82.3%. Thus, it could be seen that when considering the impact of atmospheric deposition on δ^{15}N-NH_x in the atmosphere, the contribution of agricultural sources would increase to some extent, and correspondingly, the contribution of non-agricultural sources would decrease.

Figure 3. Comparison of the source contribution ratios (top) and source contribution concentrations (bottom) of NH_4^+ in the atmosphere of the Yellow River Delta in summer of 2013 (left) and 2021 (right) from four types of NH_3 emission sources using simplified method and the fitting equation method in this study.

For the sources of NH_4^+ in the atmosphere in 2021, the most noticeable difference between the two source apportionment methods remained that the contribution proportion of fertilizer application obtained using the fitting equation method was significantly higher (30.2% by the fitting method vs. 12.5% by the simplified method) and also significantly higher for the NH_4^+ concentration in the atmosphere (1.08 $\mu g/m^3$ by the fitting method vs. 0.45 $\mu g/m^3$ by the simplified method). At the same time, the predicted contribution percentage and concentration of NH_3 emissions from livestock farming by the fitting method was much lower than those by the simple method, 17.8% and 0.64 $\mu g/m^3$for the former and 29.3% and 1.05 $\mu g/m^3$ for the latter, respectively. Thus, due to the offsetting increase and decrease in the contributions of these two types of agricultural sources to atmospheric NH_4^+ concentration, the differences in the contributions of agricultural and non-agricultural sources obtained using the two methods were not significant (agricultural sources: 41.8% using the simplified method vs. 48.0% using the fitting method; non-agricultural sources: 58.2% using the simplified method vs. 52.0% using the fitting method).

To evaluate the applicability of the proposed method in a typical urban environment, observational data of nitrogen isotopes in particulate ammonium (NH_4^+) in $PM_{2.5}$ collected in Changsha from December 2019 to October 2020 were incorporated in this study (Li et al., 2024). A Bayesian isotope mixing model was applied to quantify the contributions of ammonia sources. Except for the calculation of $\delta^{15}N_{4a\text{-}3s}$, the model structure, isotopic signatures of the four emission source categories(Table S4), and other relevant parameters were consistent with those reported by (Li et al., 2024). Aerosol samples were collected on the rooftop of a building at Central South University of Forestry and Technology (28.1°N, 113.0°E) in Changsha. The sampling site is located in a typical urban functional area, surrounded by high-density residential zones and major traffic roads, and is therefore representative of the urban atmospheric environment of Changsha.

Changsha is located in central China and is characterized by relatively flat terrain within the Xiangjiang River alluvial plain(Zhang et al., 2024; He et al., 2024). The region is subject to strong anthropogenic influences, including vehicular emissions, residential activities, and surrounding agricultural sources, leading to relatively high levels of acidic gases in the atmosphere(Zhai et al., 2014; Ma et al., 2019). According to the classification framework proposed in this study, Changsha is best categorized as the MS5 scenario, representing urban areas with relatively flat terrain and high acidic gas levels. Therefore, the fitted equation developed under the MS5 scenario was applied to calculate $\delta^{15}N_{4a\text{-}3s}$ in this simulation, in order to assess its applicability in a typical urban environment.

The simulation results indicate (Fig. 4) that, compared with the traditional 'simplified method', the use of the fitting equation developed in this study reveals that non-fossil fuel-related emissions dominate in the Changsha region, with their contribution increasing from 55.5% (agricultural emissions: 28.3 ± 13.4%, biomass combustion: 27.2 ± 14.3%) to 59.2% (agricultural emissions: 30.8 ± 21.1%, biomass combustion: 28.4 ± 22.3%). Meanwhile, the contribution from fossil fuel-related sources decreased significantly, falling from 44.5% (coal combustion: 25.5 ± 14.1%, vehicle emissions: 19.0 ± 10.5%) to

40.8% (coal combustion: 32.7 ± 24.5%, vehicle emissions: 8.1 ± 8.1%). It is worth noting that the optimised source contribution structure is closer to the NH_4^+ emission inventory for Changsha (Li et al., 2025).

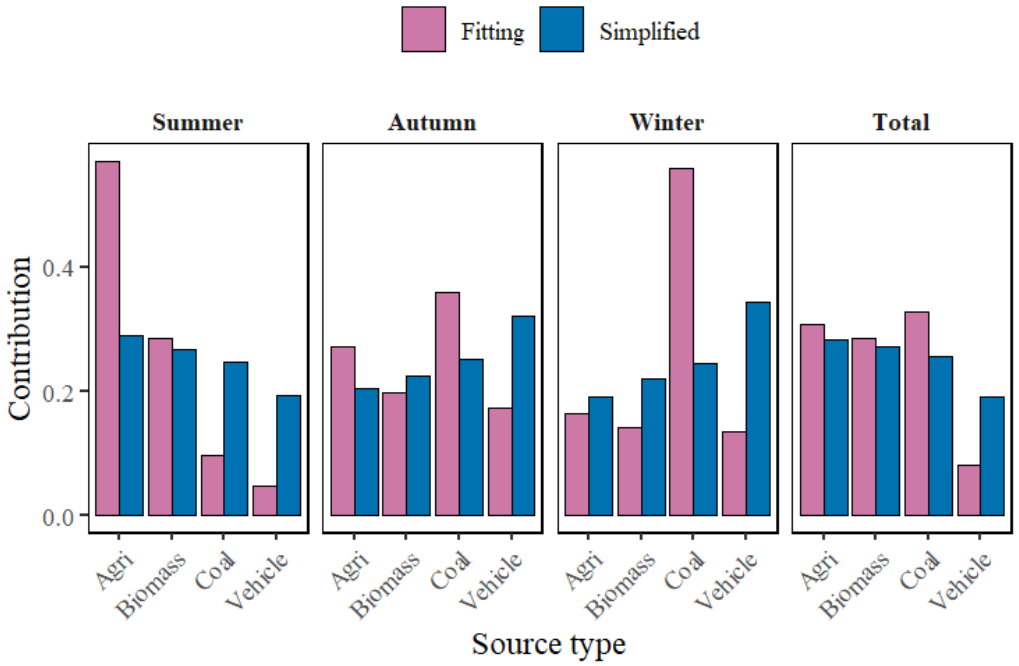

Figure 4. Comparison of source contributions ratios in Changsha from four types of NH_3 emission sources using the simplified approach and the fitted equation method developed in this study.

From a seasonal perspective, both methods indicated pronounced seasonal variations in atmospheric NH_4^+ sources in Changsha, generally characterized by an overwhelming dominance of non-fossil sources in summer and a substantial increase in fossil-fuel-related contributions in autumn and winter. In summer, agricultural emissions remained the largest source throughout. After applying the fitted equation, the contribution of agricultural emissions increased from 29.0% to 57.0%, whereas that of biomass burning decreased from 26.8% to 28.5%. The contributions from coal combustion and vehicle emissions decreased to only 9.7% and 4.8%, respectively, and the total contribution of non-fossil sources further increased from 55.8% to 85.5%. The optimized source apportionment was more consistent with emission inventory studies conducted in the Changsha–Zhuzhou–Xiangtan region and across China, which have shown that agricultural NH_3 emissions peak in summer and constitute the dominant component of regional NH_3 emissions during this season(Xu et al., 2020; Zhao et al., 2023).

Beginning in autumn, fossil-fuel-related sources gradually became dominant, and the total contributions estimated by the two methods were relatively close (simplified approach: 57.2%; fitted-equation method: 53.1%). This result is also more consistent with local observations in Changsha. Xiao et al. (2020) reported that atmospheric NH_4^+ in Changsha already exhibited a clear combustion-source dominance in autumn 2017, with fossil-fuel-related sources contributing 51.8 ± 14.9%.

Winter exhibited the strongest fossil-fuel signature, although the two methods showed marked differences in the inferred structure within fossil-related sources. The fitted equation method identified

coal combustion as the overwhelmingly dominant source in winter, with a contribution of 55.9%, substantially higher than the 24.4% estimated by the simplified approach. At the same time, the contribution of vehicle emissions was sharply reduced from 34.4% to 13.5%. According to the fitted equation method, the contributions of non-fossil and fossil sources in winter were 30.6% and 69.4%, respectively, compared with 41.2% and 58.8% derived from the simplified approach, further highlighting the dominant role of fossil-fuel emissions in winter. This interpretation is consistent with previous studies. Xu et al. (2020) and Pan et al. (2016) pointed out that winter heating increases coal consumption, leading to substantial increases in NH_4^+ and NO_3^- concentrations, and that during severe winter haze episodes, the NH_3 precursor of urban NH_4^+ is mainly controlled by fossil-fuel emissions and related industrial processes, while the influence of agricultural sources is weakened.

In the MS1 case, the difference in source contributions in 2013 was significantly greater than that in 2021, which was mainly related to the change in the atmospheric *f* value (Zong et al., 2023). Specifically, the *f* value decreased from 71.9% in 2013 to 41.6% in 2021. As shown in Fig. 1, with decreasing *f* values, the discrepancy between the simplified approach and the fitted-equation method gradually became smaller, thereby reducing the difference in source apportionment results obtained by the two methods. In contrast, the *f* value (Li et al., 2024) in MS5 was 74.6%, which was close to that of MS1 in 2013. Combined with Fig. 1, this suggests that the variation in the difference between the two methods was closely related to G_4 and D_4: when G_4 and D_4 were at relatively low levels, the difference between the two methods was comparatively small; however, in regions with higher NH_4^+ formation ratios (such as MS5 and MS6), the discrepancy between the two methods became more pronounced.

Overall, the use of experimentally validated model parameters (G_4, D_3, and D_4) can further refine the simulation results of source apportionment. Two independent cases, namely the background site MS1 and the urban site MS5, consistently demonstrated that, after accounting for atmospheric deposition, the fitted-equation method can more reasonably constrain the $\delta^{15}N_{4a\text{-}3s}$ value, thereby yielding NH_4^+ source apportionment results that are more consistent with actual regional emission characteristics. This indicates that the established fitted equation has good applicability under different environmental gradients and can significantly improve the reliability of NH_4^+ isotope-based source apportionment, thus providing a more robust tool for identifying regional ammonia emission sources and formulating emission reduction strategies.

4. Implications and Outlook

Using Bayesian mixing models to apportion sources of atmospheric NH_4^+ based on $\delta^{15}N$ data has garnered widespread attention and become a commonly applied tracing method in recent years. As the importance of this tracking method increases, this methodology is also continuously developing and improving. For instance, $\delta^{15}N\text{-}NH_3$ emitted from various sources were continuously reported and supplemented (Chang et al., 2016; Ti et al., 2021; Li et al., 2023), corrections were made for the impact of active and passive sampling on the $\delta^{15}N$ values of atmospheric NH_3 and NH_4^+ (Kawashima et al., 2021; Pan et al., 2020), quantitative assessments were conducted on equilibrium and kinetic isotopic fractionation during the gas-to-particle conversion of NH_3 to NH_4^+ in the atmosphere, and etc (Walters et al., 2019; Gu et al., 2025).

NH_3 emitted into the atmosphere undergoes continuous gas-to-particle conversion between NH_3 to NH_4^+ as it is transported and dispersed, ultimately leaving the atmospheric system primarily in the form of NH_3 to NH_4^+ through deposition. The gas-to-particle conversion process of NH_3 to NH_4^+ in the atmosphere exhibits significant isotopic fractionation, and there are marked differences in the deposition ratios of NH_3 to NH_4^+, leading to continuous changes in the atmospheric $\delta^{15}N\text{-}NH_x$ values. This change is widely recognized but has not been fully considered in the source apportionment method based on nitrogen isotope. This study developed a model to quantitatively assess the variation pattern of atmospheric $\delta^{15}N$ values under atmospheric deposition scenarios. Furthermore, a regression equation was constructed through nonlinear fitting to facilitate the application of this research finding in the tracing of atmospheric NH_4^+. Two comparative case studies revealed that using simplified methods for source apportionment of NH_4^+ could overestimate the contribution of non-agricultural sources. This understanding could partly explain the discrepancies in atmospheric ammonium sources derived from emission inventory methods and nitrogen isotope methods (Chen et al., 2022; Gu et al., 2025; Chang et al., 2019a).

The key parameters in this model (e.g., D_3, D_4, and G_4) are currently set based on a synthesis of literature values. These parameters exhibit significant spatial heterogeneity and temporal dynamics, influenced by factors such as land surface type, meteorological conditions, and atmospheric chemical composition. Future work requires multi-site, multi-season synchronous observations combining micrometeorological methods and isotopic measurements to directly obtain parameter values under different environments. This will enhance the model's empirical foundation and regional applicability.

Data availability.

The NH_4^+ data and the model developed in this study are available from the corresponding author (Chongguo Tian, cgtian@yic.ac.cn) upon reasonable request.

Author contributions.

The manuscript was written through contributions of all authors. CT designed the research, supervised the project, drafted the manuscript, and handled the submission. XHY contributed to data interpretation, figure preparation, and manuscript improvement. XNY and XT assisted with data processing and model simulations. XXY and YL contributed to method development, supported chemical analyses, and ensured data quality control. ZL and ZZ were responsible for field sampling design, sample collection logistics, and data validation. RK and YFL provided scientific consultation, helped improve the manuscript structure, and contributed to English language polishing. All authors have read and approved the final version of the manuscript.

Competing interests.

The contact author has declared that none of the authors has any competing interests.

Acknowledgements.

This work was financially supported by the Open Research Fund of Key Laboratory of Land and Sea Ecological Governance and Systematic Regulation (grant number: LSEGSR202402), and the Natural Scientific Foundation of China (grant number: 42177089, 42206240).

References

Baek, B. H. and Aneja, V. P.: Measurement and Analysis of the Relationship between Ammonia, Acid Gases, and Fine Particles in Eastern North Carolina, Journal of the Air & Waste Management Association, 54, 623-633, 10.1080/10473289.2004.10470933, 2004.

Behera, S. N. and Sharma, M.: Degradation of SO_2, NO_2 and NH_3 leading to formation of secondary inorganic aerosols: An environmental chamber study, Atmospheric Environment, 45, 4015-4024, https://doi.org/10.1016/j.atmosenv.2011.04.056, 2011.

Behera, S. N. and Sharma, M.: Transformation of atmospheric ammonia and acid gases into components of $PM_{2.5}$: an environmental chamber study, Environmental Science and Pollution Research, 19, 1187-1197, 10.1007/s11356-011-0635-9, 2012.

Behera, S. N., Sharma, M., Aneja, V. P., and Balasubramanian, R.: Ammonia in the atmosphere: a review on emission sources, atmospheric chemistry and deposition on terrestrial bodies, Environmental Science and Pollution Research, 20, 8092-8131, 10.1007/s11356-013-2051-9, 2013.

Bobbink, R., Hicks, K., Galloway, J., Spranger, T., Alkemade, R., Ashmore, M., Bustamante, M., Cinderby, S., Davidson, E., Dentener, F., Emmett, B., Erisman, J. W., Fenn, M., Gilliam, F., Nordin, A., Pardo, L., and De Vries, W.: Global assessment of nitrogen deposition effects on terrestrial plant diversity: a synthesis, Ecol. Appl., 20, 30-59, 10.1890/08-1140.1, 2010.

Bouwman, A. F., Van Vuuren, D. P., Derwent, R. G., and Posch, M.: A Global Analysis of Acidification and Eutrophication of Terrestrial Ecosystems, Water, Air, and Soil Pollution, 141, 349-382, 10.1023/a:1021398008726, 2002.

Cao, H., Liang, T., Tao, S., and Zhang, C. S.: Simulating the temporal of OCP pollution in Hangzhou, China, Chemosphere, 67, 1335–1345, 2007.

Chang, Y., Liu, X., Deng, C., Dore, A. J., and Zhuang, G.: Source apportionment of atmospheric ammonia before, during, and after the 2014 APEC summit in Beijing using stable nitrogen isotope signatures, Atmospheric Chemistry and Physics, 16, 11635-11647, 10.5194/acp-16-11635-2016, 2016.

Chang, Y., Zou, Z., Zhang, Y., Deng, C., Hu, J., Shi, Z., Dore, A. J., and Collett, J. L.: Assessing Contributions of Agricultural and Nonagricultural Emissions to Atmospheric Ammonia in a Chinese Megacity, Environmental Science & Technology, 53, 1822-1833, 10.1021/acs.est.8b05984, 2019a.

Chang, Y., Zhang, Y. L., Li, J., Tian, C., Song, L., Zhai, X., Zhang, W., Huang, T., Lin, Y. C., Zhu, C., Fang, Y., Lehmann, M. F., and Chen, J.: Isotopic constraints on the atmospheric sources and formation of nitrogenous species in clouds influenced by biomass burning, Atmospheric Chemistry and Physics, 19, 12221-12234, 10.5194/acp-19-12221-2019, 2019b.

Chen, Z.-L., Song, W., Hu, C.-C., Liu, X.-J., Chen, G.-Y., Walters, W. W., Michalski, G., Liu, C.-Q., Fowler, D., and Liu, X.-Y.: Significant contributions of combustion-related sources to ammonia emissions, Nature Communications, 13, 7710, 10.1038/s41467-022-35381-4, 2022.

Coplen, T. B.: Guidelines and recommended terms for expression of stable-isotope-ratio and gas-ratio measurement results, Rapid Communications in Mass Spectrometry, 25, 2538-2560, doi:10.1002/rcm.5129, 2011.

Dong, J., Wang, S., and Shang, K.: Simulation of the long-term transfer and fate of DDT in Lanzhou, China, Chemosphere, 81, 529-535, 2010.

Elliott, E. M., Yu, Z., Cole, A. S., and Coughlin, J. G.: Isotopic advances in understanding reactive nitrogen deposition and atmospheric processing, Science of The Total Environment, 662, 393-403, https://doi.org/10.1016/j.scitotenv.2018.12.177, 2019.

Feng, S., Xu, W., Cheng, M., Ma, Y., Wu, L., Kang, J., Wang, K., Tang, A., Collett, J. L., Jr., Fang, Y., Goulding, K., Liu, X., and Zhang, F.: Overlooked Nonagricultural and Wintertime Agricultural NH_3 Emissions in Quzhou County, North China Plain: Evidence from ^{15}N-Stable Isotopes, Environmental Science & Technology Letters, 9, 127-133, 10.1021/acs.estlett.1c00935, 2022.

Feng, Y., Su, L., Li, L., Ling, Q., Cheng, K., Lv, J., Hu, J., and Chang, Y.: Process-Based Isolation of Pyrogenic Ammonia in Urban Atmosphere and Implications for Ammonium Nitrate Control, ACS Earth and Space Chemistry, 7, 1314-1321, 10.1021/acsearthspacechem.2c00372, 2023.

Gu, M., Pan, Y., Sun, Q., Walters, W. W., Song, L., and Fang, Y.: Is fertilization the dominant source of ammonia in the urban atmosphere?, Science of The Total Environment, 838, 155890, https://doi.org/10.1016/j.scitotenv.2022.155890, 2022.

Gu, M., Zeng, Y., Walters, W. W., Sun, Q., Fang, Y., and Pan, Y.: Enhanced Nonagricultural Emissions of Ammonia Influence Aerosol Ammonium in an Urban Atmosphere: Evidence from Kinetic Versus Equilibrium Isotope Fractionation Controls on Nitrogen, Environmental Science & Technology, 59, 650-658, 10.1021/acs.est.4c09103, 2025.

He, Y., Wen, C., Fang, X., and Sun, X.: Impacts of urban-rural integration on landscape patterns and their implications for landscape sustainability: The case of Changsha, China, Landscape Ecology, 39, 129, 10.1007/s10980-024-01926-9, 2024.

Hu, Q., Zhang, L., Evans, G. J., and Yao, X.: Variability of atmospheric ammonia related to potential emission sources in downtown Toronto, Canada, Atmospheric Environment, 99, 365-373, http://dx.doi.org/10.1016/j.atmosenv.2014.10.006, 2014.

Ianniello, A., Spataro, F., Esposito, G., Allegrini, I., Rantica, E., Ancora, M. P., Hu, M., and Zhu, T.: Occurrence of gas phase ammonia in the area of Beijing (China), Atmospheric Chemistry and Physics, 10, 9487-9503, 10.5194/acp-10-9487-2010, 2010.

Kawashima, H. and Ono, S.: Nitrogen Isotope Fractionation from Ammonia Gas to Ammonium in Particulate Ammonium Chloride, Environmental Science & Technology, 53, 10629-10635, 10.1021/acs.est.9b01569, 2019.

Kawashima, H., Ogata, R., and Gunji, T.: Laboratory-based validation of a passive sampler for determination of the nitrogen stable isotope ratio of ammonia gas, Atmospheric Environment, 245, 118009, https://doi.org/10.1016/j.atmosenv.2020.118009, 2021.

Kim, T.-W., Lee, K., Najjar, R. G., Jeong, H.-D., and Jeong, H. J.: Increasing N Abundance in the Northwestern Pacific Ocean Due to Atmospheric Nitrogen Deposition, Science, 334, 505-509, 10.1126/science.1206583, 2011.

Li, B., Chen, L., Shen, W., Jin, J., Wang, T., Wang, P., Yang, Y., and Liao, H.: Improved gridded ammonia emission inventory in China, Atmospheric Chemistry and Physics, 21, 15883-15900, 10.5194/acp-21-15883-2021, 2021.

Li, D., Liu, H., and Duan, G.: High-resolution anthropogenic emission inventory for China (2015–2024): Spatiotemporal changes and environmental application, Atmospheric Environment, 361, 121495, https://doi.org/10.1016/j.atmosenv.2025.121495, 2025.

Li, L., Lollar, B. S., Li, H., Wortmann, U. G., and Lacrampe-Couloume, G.: Ammonium stability and nitrogen isotope fractionations for $-NH_3(aq)-NH_3(gas)$ systems at 20–70 °C and pH of 2–13: Applications to habitability and nitrogen cycling in low-temperature hydrothermal systems, Geochimica et Cosmochimica Acta, 84, 280-296, http://dx.doi.org/10.1016/j.gca.2012.01.040, 2012.

Li, Y., Huang, S., and Han, M.: An assessment of the factors that drive changes in the distribution and area of cultivated land in the Yellow River Delta, China, Environmental Earth Sciences, 81, 227, 10.1007/s12665-022-10347-3, 2022.

Li, Y., Liu, J., George, C., Herrmann, H., Gu, M., Yang, M., Wang, Y., Mellouki, A., Pan, Y., Felix, J. D., Kawashima, H., Zhang, Z., Wang, S., and Zeng, Y.: Apportioning Atmospheric Ammonia Sources across Spatial and Seasonal Scales by Their Isotopic Fingerprint, Environmental Science & Technology, 57, 16424-16434, 10.1021/acs.est.3c04027, 2023.

Li, Z., Xiao, H., Walters, W. W., Hastings, M. G., Min, J., Song, L., Lu, W., Wu, L., Yan, W., Liu, S., and Fang, Y.: Nitrogen isotopic characteristics of aerosol ammonium in a Chinese megacity indicate the reduction from vehicle emissions during the lockdown period, Science of The Total Environment, 922, 171265, https://doi.org/10.1016/j.scitotenv.2024.171265, 2024.

Liu, M., Huang, X., Song, Y., Tang, J., Cao, J., Zhang, X., Zhang, Q., Wang, S., Xu, T., Kang, L., Cai, X., Zhang, H., Yang, F., Wang, H., Yu, J. Z., Lau, A. K. H., He, L., Huang, X., Duan, L., Ding, A., Xue, L., Gao, J., Liu, B., and Zhu, T.: Ammonia emission control in China would mitigate haze pollution and nitrogen deposition, but worsen acid rain, Proceedings of the National Academy of Sciences, 116, 7760-7765, 10.1073/pnas.1814880116, 2019.

Ma, X., Xiao, Z., He, L., Shi, Z., Cao, Y., Tian, Z., Vu, T., and Liu, J.: Chemical Composition and Source Apportionment of $PM_{2.5}$ in Urban Areas of Xiangtan, Central South China, International Journal of Environmental Research and Public Health, 16, 539, 2019.

Pan, Y., Tian, S., Liu, D., Fang, Y., Zhu, X., Zhang, Q., Zheng, B., Michalski, G., and Wang, Y.: Fossil fuel combustion-related emissions dominate atmospheric ammonia sources during severe haze episodes:

Evidence from ^{15}N-stable isotope in size-resolved aerosol ammonium, Environmental Science & Technology, 50, 8049–8056, 10.1021/acs.est.6b00634, 2016.

Pan, Y., Tian, S., Liu, D., Fang, Y., Zhu, X., Gao, M., Wentworth, G. R., Michalski, G., Huang, X., and Wang, Y.: Source Apportionment of Aerosol Ammonium in an Ammonia-Rich Atmosphere: An Isotopic Study of Summer Clean and Hazy Days in Urban Beijing, Journal of Geophysical Research: Atmospheres, 123, 5681-5689, doi:10.1029/2017JD028095, 2018.

Pan, Y., Gu, M., Song, L., Tian, S., Wu, D., Walters, W. W., Yu, X., Lü, X., Ni, X., Wang, Y., Cao, J., Liu, X., Fang, Y., and Wang, Y.: Systematic low bias of passive samplers in characterizing nitrogen isotopic composition of atmospheric ammonia, Atmospheric Research, 243, 105018, https://doi.org/10.1016/j.atmosres.2020.105018, 2020.

Schiferl, L. D., Heald, C. L., Van Damme, M., Clarisse, L., Clerbaux, C., Coheur, P. F., Nowak, J. B., Neuman, J. A., Herndon, S. C., Roscioli, J. R., and Eilerman, S. J.: Interannual variability of ammonia concentrations over the United States: sources and implications, Atmospheric Chemistry and Physics, 16, 12305-12328, 10.5194/acp-16-12305-2016, 2016.

Schrader, F. and Brummer, C.: Land Use Specific Ammonia Deposition Velocities: a Review of Recent Studies (2004-2013), Water Air and Soil Pollution, 225, 2114-2125, 10.1007/s11270-014-2114-7, 2014.

Shen, J., Liu, X., Zhang, Y., Fangmeier, A., Goulding, K., and Zhang, F.: Atmospheric ammonia and particulate ammonium from agricultural sources in the North China Plain, Atmospheric Environment, 45, 5033-5041, http://dx.doi.org/10.1016/j.atmosenv.2011.02.031, 2011.

Shen, J. L., Tang, A. H., Liu, X. J., Fangmeier, A., Goulding, K. T. W., and Zhang, F. S.: High concentrations and dry deposition of reactive nitrogen species at two sites in the North China Plain, Environmental Pollution, 157, 3106-3113, http://dx.doi.org/10.1016/j.envpol.2009.05.016, 2009.

Sui, X., Yang, L.-X., Yi, H., Yuan, Q., Yan, C., Dong, C., Meng, C.-P., Yao, L., Yang, F., and Wang, W.-X.: Influence of Seasonal Variation and Long-Range Transport of Carbonaceous Aerosols on Haze Formation at a Seaside Background Site, China, Aerosol and Air Quality Research, 15, 1251-1260, 10.4209/aaqr.2014.09.0185, 2015.

Sun, K., Tao, L., Miller, D. J., Pan, D., Golston, L. M., Zondlo, M. A., Griffin, R. J., Wallace, H. W., Leong, Y. J., Yang, M. M., Zhang, Y., Mauzerall, D. L., and Zhu, T.: Vehicle Emissions as an Important Urban Ammonia Source in the United States and China, Environmental Science & Technology, 10.1021/acs.est.6b02805, 2016.

Sun, X., Zong, Z., Li, Q., Shi, X., Wang, K., Lu, L., Li, B., Qi, H., and Tian, C.: Assessing the emission sources and reduction potential of atmospheric ammonia at an urban site in Northeast China, Environmental Research, 198, 111230, https://doi.org/10.1016/j.envres.2021.111230, 2021.

Sun, Z., Zong, Z., Tan, Y., Tian, C., Liu, Z., Zhang, F., Sun, R., Chen, Y., Li, J., and Zhang, G.: Characterization of the nitrogen stable isotope composition ($\delta^{15}N$) of ship-emitted NOx, Atmospheric Chemistry and Physics, 23, 12851-12865, 10.5194/acp-23-12851-2023, 2023.

Tan, J., Fu, J. S., and Seinfeld, J. H.: Ammonia emission abatement does not fully control reduced forms of nitrogen deposition, Proceedings of the National Academy of Sciences, 117, 9771-9775, 10.1073/pnas.1920068117, 2020.

Ti, C., Ma, S., Peng, L., Tao, L., Wang, X., Dong, W., Wang, L., and Yan, X.: Changes of $\delta^{15}N$ values during the volatilization process after applying urea on soil, Environmental Pollution, 270, 116204, https://doi.org/10.1016/j.envpol.2020.116204, 2021.

Urey, H.: The thermodynamic properties of isotopic substances, Journal of the Chemical Society, 562-581, 1947.

Walters, W. W., Chai, J., and Hastings, M. G.: Theoretical Phase Resolved Ammonia–Ammonium Nitrogen Equilibrium Isotope Exchange Fractionations: Applications for Tracking Atmospheric Ammonia Gas-to-Particle Conversion, ACS Earth and Space Chemistry, 3, 79-89, 10.1021/acsearthspacechem.8b00140, 2019.

Wang, S., Ren, Y., Xia, B., Liu, K., and Li, H.: Prediction of atmospheric pollutants in urban environment based on coupled deep learning model and sensitivity analysis, Chemosphere, 331, 138830, https://doi.org/10.1016/j.chemosphere.2023.138830, 2023.

Xiao, H.-W., Wu, J.-F., Luo, L., Liu, C., Xie, Y.-J., and Xiao, H.-Y.: Enhanced biomass burning as a source of aerosol ammonium over cities in central China in autumn, Environmental Pollution, 266, 115278, https://doi.org/10.1016/j.envpol.2020.115278, 2020.

Xu, B., You, X., Zhou, Y., Dai, C., Liu, Z., Huang, S., Luo, D., and Peng, H.: The Study of Emission Inventory on Anthropogenic Air Pollutants and Source Apportionment of $PM_{2.5}$ in the Changzhutan Urban Agglomeration, China, 10.3390/atmos11070739, 2020.

Xu, S.: Predicted Residual Error Sum of Squares of Mixed Models: An Application for Genomic Prediction, G3 Genes|Genomes|Genetics, 7, 895-909, 10.1534/g3.116.038059, 2017.

Zhai, Y., Liu, X., Chen, H., Xu, B., Zhu, L., Li, C., and Zeng, G.: Source identification and potential ecological risk assessment of heavy metals in $PM_{2.5}$ from Changsha, Science of The Total Environment, 493, 109-115, https://doi.org/10.1016/j.scitotenv.2014.05.106, 2014.

Zhang, B., Fan, J., Zhang, P., Shen, S., and Ren, Y.: The Changsha historic urban area: a study on the evolution characteristics and influencing factors of the connectivity of construction land, Heritage Science, 12, 287, 10.1186/s40494-024-01401-3, 2024.

Zhang, L., Gong, S., Padro, J., and Barrie, L.: A size-segregated particle dry deposition scheme for an atmospheric aerosol module, Atmospheric Environment, 35, 549-560, 2001.

Zhang, X., Zuo, L., Lu, Y., Li, H., and Zhao, Y.: An improved approach for retrieval of tidal flat elevation based on inundation frequency, Estuarine, Coastal and Shelf Science, 313, 109061, https://doi.org/10.1016/j.ecss.2024.109061, 2025.

Zhang, Y., Benedict, K. B., Tang, A., Sun, Y., Fang, Y., and Liu, X.: Persistent Nonagricultural and Periodic Agricultural Emissions Dominate Sources of Ammonia in Urban Beijing: Evidence from ^{15}N Stable Isotope in Vertical Profiles, Environmental Science & Technology, 54, 102-109, 10.1021/acs.est.9b05741, 2020.

Zhang, Y., Ma, X., Tang, A., Fang, Y., Misselbrook, T., and Liu, X.: Source Apportionment of Atmospheric Ammonia at 16 Sites in China Using a Bayesian Isotope Mixing Model Based on $\delta^{15}N$–NHx Signatures, Environmental Science & Technology, 57, 6599-6608, 10.1021/acs.est.2c09796, 2023.

Zhang, Y., Dore, A. J., Ma, L., Liu, X. J., Ma, W. Q., Cape, J. N., and Zhang, F. S.: Agricultural ammonia emissions inventory and spatial distribution in the North China Plain, Environmental Pollution, 158, 490-501, http://dx.doi.org/10.1016/j.envpol.2009.08.033, 2010.

Zhao, Y., Zhang, L., Chen, Y., Liu, X., Xu, W., Pan, Y., and Duan, L.: Atmospheric nitrogen deposition to China: A model analysis on nitrogen budget and critical load exceedance, Atmospheric Environment, 153, 32-40, http://dx.doi.org/10.1016/j.atmosenv.2017.01.018, 2017.

Zhao, Y., Li, B., Dong, J., Li, Y., Wang, X., Gan, C., Lin, Y., and Liao, H.: Improved ammonia emission inventory of fertilizer application for three major crops in China based on phenological data, Science of The Total Environment, 896, 165225, https://doi.org/10.1016/j.scitotenv.2023.165225, 2023.

Zhu, C., Li, R., Qiu, M., Zhu, C., Gai, Y., Li, L., Yang, N., Sun, L., Wang, C., Wang, B., Yan, G., and Xu, C.: High spatiotemporal resolution ammonia emission inventory from typical industrial and agricultural province of China from 2000 to 2020, Science of The Total Environment, 918, 170732, 10.1016/j.scitotenv.2024.170732, 2024.

Zong, Z., Chen, Y., Tian, C., Fang, Y., Wang, X., Huang, G., Zhang, F., Li, J., and Zhang, G.: Radiocarbon-based impact assessment of open biomass burning on regional carbonaceous aerosols in North China, Science of The Total Environment, 518–519, 1-7, 10.1016/j.scitotenv.2015.01.113, 2015.

Zong, Z., Ren, C., Shi, X., Sun, Z., Huang, X., Tian, C., Li, J., Zhang, G., Fang, Y., and Gao, H.: Isotopic comparison of ammonium between two summertime field campaigns in 2013 and 2021 at a background site of North China, Science of The Total Environment, 905, 167304, https://doi.org/10.1016/j.scitotenv.2023.167304, 2023.